A&A 439, 539–550 (2005)
DOI: 10.1051/0004-6361:20041685

Astronomy & Astrophysics

ISO observations of the Wolf-Rayet galaxies NGC 5430, NGC 6764, Mrk 309 and VII Zw 19⋆

B. O'Halloran[1,2,3], B. McBreen[3], L. Metcalfe[4], M. Delaney[3], and D. Coia[3]

[1] Dunsink Observatory, Castleknock, Dublin 15, Ireland
e-mail: boh@physics.gmu.edu
[2] Dept. of Physics and Astronomy, George Mason University, Fairfax, Virginia, 22030, USA
[3] Physics Department, University College, Belfield, Dublin 4, Ireland
[4] XMM-Newton Science Operations Centre, European Space Agency, Villafranca del Castillo, PO Box 50727, 28080 Madrid, Spain

Received 19 July 2004 / Accepted 10 May 2005

Abstract. Observations of four WR galaxies (NGC 5430, NGC 6764, Mrk 309 and VII Zw 19) using the Infrared Space Observatory are presented here. ISOCAM maps of NGC 5430, Mrk 309 and NGC 6764 revealed the location of star formation regions in each of these galaxies. ISOPHOT spectral observations from 4 to 12 μm detected the ubiquitous PAH bands in the nuclei of the targets and several of the disk star forming regions, while LWS spectroscopy detected [O I] and [C II] emission lines from two galaxies, NGC 5430 and NGC 6764.
Using a combination of ISO and IRAS flux densities, a dust model based on the sum of modified blackbody components was successfully fitted to the available data. These models were then used to calculate new values for the total IR luminosities for each galaxy, the size of the various dust populations, and the global SFR.
The derived flux ratios, the SFRs, the high L(PAH)/L(40–120 μm) and F(PAH 7.7 μm)/F(7.7 μm continuum) values suggest that most of these galaxies are home to only a compact burst of star formation. The exception is NGC 6764, whose F(PAH 7.7 μm)/F(7.7 μm continuum) value of 1.22 is consistent with the presence of an AGN, yet the L(PAH)/L(40–120 μm) is more in line with a starburst, a finding in line with a compact low-luminosity AGN dominated by the starburst.

Key words. stars: Wolf-Rayet – galaxies: active – infrared: galaxies – galaxies: interactions – galaxies: starburst

1. Introduction

1.1. WR galaxies

Wolf-Rayet (WR) galaxies are defined as those galaxies whose integrated spectra contain a broad emission feature at HeII λ4686 (Conti 1991). This feature has a full-width half-max (*FWHM*) of about 10–20 Å and is a typical signature of WR stars. Though Seyfert galaxies and active galactic nuclei (AGN) often show a HeII λ4686 emission line, WR galaxies can be distinguished from them by their relatively narrow nebular emission lines. WR galaxies are found exclusively among emission line (EL) galaxies, where the photoionization of the nebular line is stellar in origin, and also possess a very blue continuum which is indicative of a large population of young hot massive stars. The broad HeII λ4686 emission feature is very prominent in the spectra of Galactic and LMC WR stars. By comparing the luminosity and width of this feature as it appears in the spectrum of a WR galaxy, with the corresponding emission lines from Galactic WR stars, an estimate of the number of WR stars in a WR galaxy can be made.

The first galaxy in which this WR feature was discovered (Allen et al. 1976) was the blue compact dwarf He 2–10, though NGC 6764 and Mrk 309 were the first objects to be actually referred to as WR galaxies (Osterbrock & Cohen 1982). The first comprehensive catalogue was compiled by Conti (1991), and included approximately 40 galaxies. Since then, the number of known WR galaxies has grown rapidly to more than 130. These have been most recently catalogued by Schaerer et al. (1999). Many of the new members of this catalogue show additional features from WR stars in their spectra. For example, the broad emission lines of NIII λ4640 and/or CIII λ4650 as well as CIV λ5808 are among the strongest optical lines in WN and WC stars and are increasingly being detected.

WR galaxies are found among a large variety of morphological types, from low-mass blue compact dwarfs and irregular galaxies, to massive spirals and luminous merging

⋆ Based on observations with ISO, an ESA project with instruments funded by ESA Member States (especially the PI countries: France, Germany, The Netherlands and the UK) with the participation of ISAS and NASA.

IRAS galaxies. There are systems where WR stars are found in singular giant HII regions (e.g. Tol 89 within the galaxy NGC 5398), in the nucleus or core (e.g. in the barred spiral LINER NGC 6764), in knots (e.g. at the end of the bar in the barred spiral NGC 5430) and in interacting members of compact groups (e.g. HCG 31A and C) (O'Halloran et al. 2002). Given the wide range of morphological types, an age ≤ 10 Myr and high initial masses of $M_{\rm ini} \geq 35\ M_{\odot}$ (Maeder & Conti 1994), WR galaxies are therefore ideal objects to study the early phases of starbursts, determine burst properties (age, duration, SFR) and to constrain parameters (i.e. slope and upper mass cut-off) of the upper part of the initial mass function. Conversely studies of the stellar populations in super star clusters frequently formed in starbursts and WR galaxies (Conti & Vacca 1994; Meurer et al. 1995) can also place constraints on stellar evolution models for massive stars (e.g. at extremely low metallicities) which are inaccessible in the Local Group.

1.2. Why observe WR galaxies with ISO?

Observations of four out of six WR galaxies which were part of the ISO WRHIIGAL program (O'Halloran et al. 2000, 2002) are presented in this paper, along with supplemental archival observations from the IRGAL_1 (PI: Tonaka), GALXISM (PI: Smith), MPEXGAL1 (PI: Genzel) and WMFP15_A (PI: Wozniak) programs. The main goal of the original WRHIIGAL program was to systematically investigate a sample of WR galaxies in order to try to understand what induces such a massive burst of star formation in these systems, and to investigate the mid and far-IR characteristics of such objects. The fact that WR galaxies are roughly a coeval sample makes comparisons with other starburst galaxies important. Given the importance of the mid-infrared region of the spectrum for the physics of star formation and for exploring the links between massive star formation in galaxies and AGN, acquisition of data in this wavelength range was crucial. However, no other instruments prior to the launch of ISO could provide spatially and spectrally resolved mid-infrared data on a sample of WR and starburst galaxies – ISO data was crucial in opening up this important area of research, such as those obtained using mid-IR data from surveys of starburst and blue compact galaxies in the ISO WRHIIGAL and HAROA programs (Steel et al. 1996; O'Halloran et al. 2000, 2002; Metcalfe et al. 2005; O'Halloran et al. 2005). The ISOCAM, ISOPHOT and LWS observations provided maps and spectra of the galaxies in one, or in combinations of, the Unidentified Infrared Bands (UIB) and dust or nebular line emission. They enabled a determination of the spatial relationship between the optical star forming regions and the infrared emission from the young WR and starburst regions, allowing a discrimination of the relative contribution to the infrared flux from dust, nebular emission and polycyclic aromatic hydrocarbon (PAH) molecules. The advent of the Spitzer Space Telescope, optimized to conduct research in a similar wavelength range but with greater spatial and spectral resolution, will further open up this research field over the forthcoming years.

Table 1. Characteristics and parameters of the WR galaxy sample. The four columns give the galaxy name, alternative designations, morphological type and distance in Mpc, assuming $H_0 = 75$ km s^{-1} Mpc^{-1}.

Galaxy	Other designations	Morphology	Distance [Mpc]
NGC 5430	Mrk 799	SB(s)b HII	39.8
NGC 6764	UGC 11407	SB(s)bc; LINER Sy2	32.4
Mrk 309	IV Zw 121	Sa Sy2 HII	174.1
VII Zw 19	PGC 015803	–	65.2

1.3. The sample of WR galaxies

Four galaxies displaying WR features were observed, as part of a wider survey of starburst and WR galaxies (the WRHIIGAL and HAROA programs) (Steel et al. 1996; O'Halloran et al. 2000, 2002; Metcalfe et al. 2005; O'Halloran et al. 2005) by the Infrared Space Observatory, are discussed in this section. Table 1 lists the basic properties of each galaxy.

1.3.1. NGC 5430

NGC 5430 (Mrk 799) is a nearby S-shaped barred spiral galaxy (SBb) located at a distance of 39.8 Mpc. Keel (1982) detected the broad 4650 Å emission feature in the knot southeast of the nucleus, at the end of the bar. This knot is an extremely luminous HII region (Keel 1982, 1987) though of unusually low luminosity at 4.885 GHz (Condon et al. 1982), possibly indicating an anomalously low supernova rate.

1.3.2. NGC 6764

At a distance of 32.4 Mpc, NGC 6764 is a nearby S-shaped barred spiral galaxy (SBbc), somewhat similar to NGC 5430. Originally considered to be a Seyfert 2 galaxy by Rubin et al. (1975), Heckman (1980) later classified NGC 6764 as a LINER on account of its large OI λ6300/OIII λ5007 ratio of ~0.3. This galaxy contains a nuclear stellar optical continuum source which extends over ~1.6″ (Rubin et al. 1975).

1.3.3. Mrk 309

At a distance of 174.1 Mpc, Mrk 309 is the most distant object in the sample. It was identified as a galaxy with a bright UV continuum, noticeable Hα emission and possible Seyfert characteristics (Markarian & Lipovetskii 1971).

Mrk 309 appears in the sample of 212 emission-line galaxies extracted from the Universidad Complutense de Madrid (UCM) lists (Zamorano et al. 1994) and was described as a Wolf-Rayet dominated nucleus galaxy with various HII regions outside the nucleus. The *R*-band image of Mrk 309 presented by Vitores et al. (1996) shows that the southern arm is more prominent than the northern and ends in a knot approximately 12″ from the nucleus.

1.3.4. VII Zw 19

VII Zw 19 appears in the list of WR galaxies discovered by Kunth & Joubert (1985) from a search among a sample of 45 blue EL galaxies. A broad emission band between 4600 Å and 4711 Å was the criteria used to decide that this EL galaxy is also a WR galaxy. Beck (2000) notes that the radio and Hα emission from this galaxy have the same basic structure of a very strong central source embedded in a weak envelope. The central non-thermal source appears to be unresolved and is about 800 times more luminous than Cas A. Recent MERLIN and VLA observations (Beck et al. 2004) note that VII Zw 19 resembles M 82 in its radio and infrared spectrum, however the starburst region of VII Zw 19 is twice the size and twice as luminous as that of M 82. VII Zw 19 is situated at a distance of 65.2 Mpc.

We present ISOCAM, ISOPHOT and LWS observations of these galaxies as part of an observing program consisting of several galaxies exhibiting Wolf-Rayet signatures. The observations and data reduction are presented in Sect. 2. The results are contained in Sect. 3 and discussed in Sect. 4. The conclusions are summarized in Sect. 5.

2. Observations and data reduction

The ISO (Kessler et al. 2003) observations were obtained using the mid-infrared camera ISOCAM (Blommaert et al. 2003), the spectrometric mode of the ISO photopolarimeter ISOPHOT (Laureijs et al. 2003a) and the medium-resolution grating mode of the long wavelength spectrometer LWS (Gry et al. 2003). The astronomical observing template (AOT) used numbers and the observing log for the ISO observations is presented in Table 2.

2.1. ISOCAM

The observations had the following configuration: 1.5, 3 and 6″ PFOV (for Mrk 309 $LW2/LW3$, NGC 5430 and NGC 6764 $LW2/LW3$ and $LW10$ observations respectively), integration time of 2.1 s and ∼100 readouts (excluding discarded stabilisation readouts). The diameter of the point spread function (PSF) central maximum at the first Airy minimum is $0.84 \times \lambda(\mu\mathrm{m})$ arcseconds. The *FWHM* is about half that amount. A discussion of the data reduction steps for the CAM data can be found in O'Halloran et al. (2002).

2.2. PHT-S

PHT-S consists of a dual grating spectrometer with a resolving power of 90 (Laureijs et al. 2003b). Band SS covers the range 2.5–4.8 μm, while band SL covers the range 5.8–11.6 μm. Two different chopping modes were used. The NGC 5430 and Mrk 309 PHT-S spectra were obtained by pointing the 24″ × 24″ aperture of PHT-S alternatively towards the peak of the emission (for 512 s) and then towards two background positions off the galaxy (256 s each), using the ISOPHOT focal plane chopper. The NGC 6764 and VII Zw 19 PHT-S spectra were obtained on the other hand by operating the PHT-S aperture in rectangular chopping mode. The satellite pointed to a position between the source and an off-source position, and the chopper moved then alternatively between these two positions. The source was always in the positive beam in the spacecraft Y-direction. The calibration of the spectra was performed by using a spectral response function derived from several calibration stars of different brightness observed in chopper mode (Acosta-Pulido et al. 2000). The relative spectrometric uncertainty of the PHT-S spectrum is about 20% when comparing different parts of the spectrum that are more than a few microns apart. The absolute photometric uncertainty is ≤10% for bright calibration sources. A discussion of the data reduction steps for the PHOT data can be found in O'Halloran et al. (2002).

2.3. LWS

The LWS spectra were obtained with the aperture centered on the 6.7 μm ISOCAM map for NGC 5430 and on the nuclear region of the galaxy for NGC 6764. It was assumed that for both objects the source was completely included in the beam of the LWS instrument, so that no extended-source correction was necessary. The beam of LWS was slightly elliptical and its *FWHM* varied between 65″ and 85″, depending on wavelength and direction (Swinyard et al. 1998). The grating was fully scanned 6 times over the entire wavelength range. A spectral sampling interval of 4 was employed to give 4 spectral points per resolution element in each of the scans. All the datasets were first processed with version 10 of the LWS pipeline processing software, OLP V10.1 (Gry et al. 2003). The LWS Interactive Analysis package LIA (Sidher et al. 1997) was then used to further process the output of the standard pipeline. The nominal, fixed, dark current values, as determined from the dedicated measurements in revolution 650 (Swinyard et al. 2000) were subtracted from the data. The data was rebinned to one point per LWS detector, employing a scan-averaging method described by Sidher et al. (2000), yielding 10 bandpass continuum estimates spanning the LWS spectral range, and are plotted in Fig. 3.

3. Results

3.1. ISOCAM maps

3.1.1. NGC 5430

Deconvolved 6.7, 12 and 14.3 μm maps of NGC 5430 overlaid on a DSS image are presented in Figs. 1(I), (II) and (III) respectively. It can clearly be seen that the ISOCAM contours follow the general form of the galaxy, especially on the 12 μm map. In addition three sources were clearly detected in the higher resolution 12 μm map and are labelled A, B and N, though source B was also detected at 6.7 and 14.3 μm. The source B coincides with the highly luminous southeast HII region and contains the majority of the WR population. The weaker source A is probably associated with a less luminous HII region in NGC 5430. The nucleus of NGC 5430 is denoted N in Fig. 1(II). The derived fluxes for NGC 5430 are given in Table 3.

Table 2. Log of the ISO observations for the four galaxies. The 14 columns list the object, the TDT number (a unique identifier of an ISO observation), the proposal name, the AOT number (which identified the observing mode used), the filter, the wavelength range ($\Delta\lambda$), the reference wavelength of the filter, the FOV, the duration of the observation, and the center of the instrument field of view in right ascension and declination respectively.

Target	TDT	Proposal	AOT	Filter/Mode	$\Delta\lambda$	$\lambda_{\rm ref}$	FOV	MxN raster	Δ step	BmSw	Duration	Right Ascension	Declination
				(μm)	(μm)	(arcsec)	(arcsec)		dM (arcsec) dN(arcsec)	(arcsec)	(s)	(RA)	(Dec)
NGC 5430	IRGAL_1	33700518	CAM01	*LW*2	5.0–8.0	6.75	384 × 384	3 × 3	96 96	N/A	393	$14^{\rm h}00^{\rm m}45.6^{\rm s}$	59°19′44.0″
	IRGAL_1	33700518	CAM01	*LW*3	12.0–18.0	14.3	384 × 384	3 × 3	96 96	N/A	300	$14^{\rm h}00^{\rm m}45.6^{\rm s}$	50°19′44.0″
	WRHIIGAL	51400519	CAM01	*LW*10	8.0–15.0	12.0	168 × 144	4 × 3	96 96	N/A	1022	$14^{\rm h}00^{\rm m}47.4^{\rm s}$	59°19′26.5″
	WRHIIGAL	51400215	PHT40	SS/SL	2.5–11.6	–	24 × 24	N/A	N/A	tri150	1132	$14^{\rm h}00^{\rm m}44.6^{\rm s}$	59°19′57.2″
	WRHIIGAL	51400313	PHT40	SS/SL	2.5–11.6	–	24 × 24	N/A	N/A	tri150	1132	$14^{\rm h}00^{\rm m}45.8^{\rm s}$	59°19′43.6″
	WRHIIGAL	51400414	PHT40	SS/SL	2.5–11.6	–	24 × 24	N/A	N/A	tri150	1132	$14^{\rm h}00^{\rm m}47.4^{\rm s}$	59°19′26.5″
	IRGAL_1	51400417	LWS01	–	43.0–190.0	–	101	N/A	N/A		2124	$14^{\rm h}00^{\rm m}45.6^{\rm s}$	59°19′43.9″
	IRGAL_1	51400416	LWS01	–	43.0–190.0	–	101	N/A	N/A	subtr off	2126	$14^{\rm h}00^{\rm m}45.3^{\rm s}$	59°26′43.9″
NGC 6764	WMFP15_A	69301328	CAM03	*LW*2	5.0–8.0	6.75	48 × 48	N/A	N/A	600	2438	$19^{\rm h}08^{\rm m}16.4^{\rm s}$	50°55′59.6″
	WMFP15_A	69301328	CAM03	*LW*3	12.0–18.0	14.3	48 × 48	N/A	N/A	600	2438	$19^{\rm h}08^{\rm m}16.4^{\rm s}$	50°55′59.6″
	WRHIIGAL	75301710	CAM01	*LW*10	8.0–15.0	12.0	168 × 132	4 × 4	24 12	N/A	2126	$19^{\rm h}08^{\rm m}16.4^{\rm s}$	50°55′58.5″
	MPEXGAL1	63801718	PHT40	SS/SL	2.5–11.6	–	24 × 24	N/A	N/A	rect060	1132	$19^{\rm h}08^{\rm m}16.4^{\rm s}$	50°55′59.4″
	WRHIIGAL	74501017	PHT40	SS/SL	2.5–11.6	–	24 × 24	N/A	N/A	rect060	1132	$19^{\rm h}08^{\rm m}12.8^{\rm s}$	50°55′48.8″
	WRHIIGAL	11601781	PHT40	SS/SL	2.5–11.6	–	24 × 24	N/A	N/A	180	1132	$19^{\rm h}08^{\rm m}21.5^{\rm s}$	50°55′56.8″
	GALXISM	30200964	LWS01	–	43.0–190.0	–	84	N/A	N/A		1920	$19^{\rm h}08^{\rm m}16.3^{\rm s}$	50°55′59.5″
Mrk 309	WRHIIGAL	55100531	CAM03	*LW*3	12.0–18.0	14.3	48 × 48	N/A	N/A	60	1010	$22^{\rm h}52^{\rm m}34.7^{\rm s}$	24°43′49.5″
	WRHIIGAL	55100433	CAM03	*LW*6	7.0–8.5	7.7	48 × 48	N/A	N/A	60	1220	$22^{\rm h}52^{\rm m}34.7^{\rm s}$	24°43′49.5″
	WRHIIGAL	55100306	PHT40	SS/SL	2.5–11.6	–	24 × 24	N/A	N/A	tri090	1132	$22^{\rm h}52^{\rm m}34.7^{\rm s}$	24°43′49.0″.
VII Zw 19	WRHIIGAL	63702104	PHT40	SS/SL	2.5–11.6	–	24 × 24	n/a	n/a	rect030	1132	$04^{\rm h}40^{\rm m}39.3^{\rm s}$	67°44′20.0″

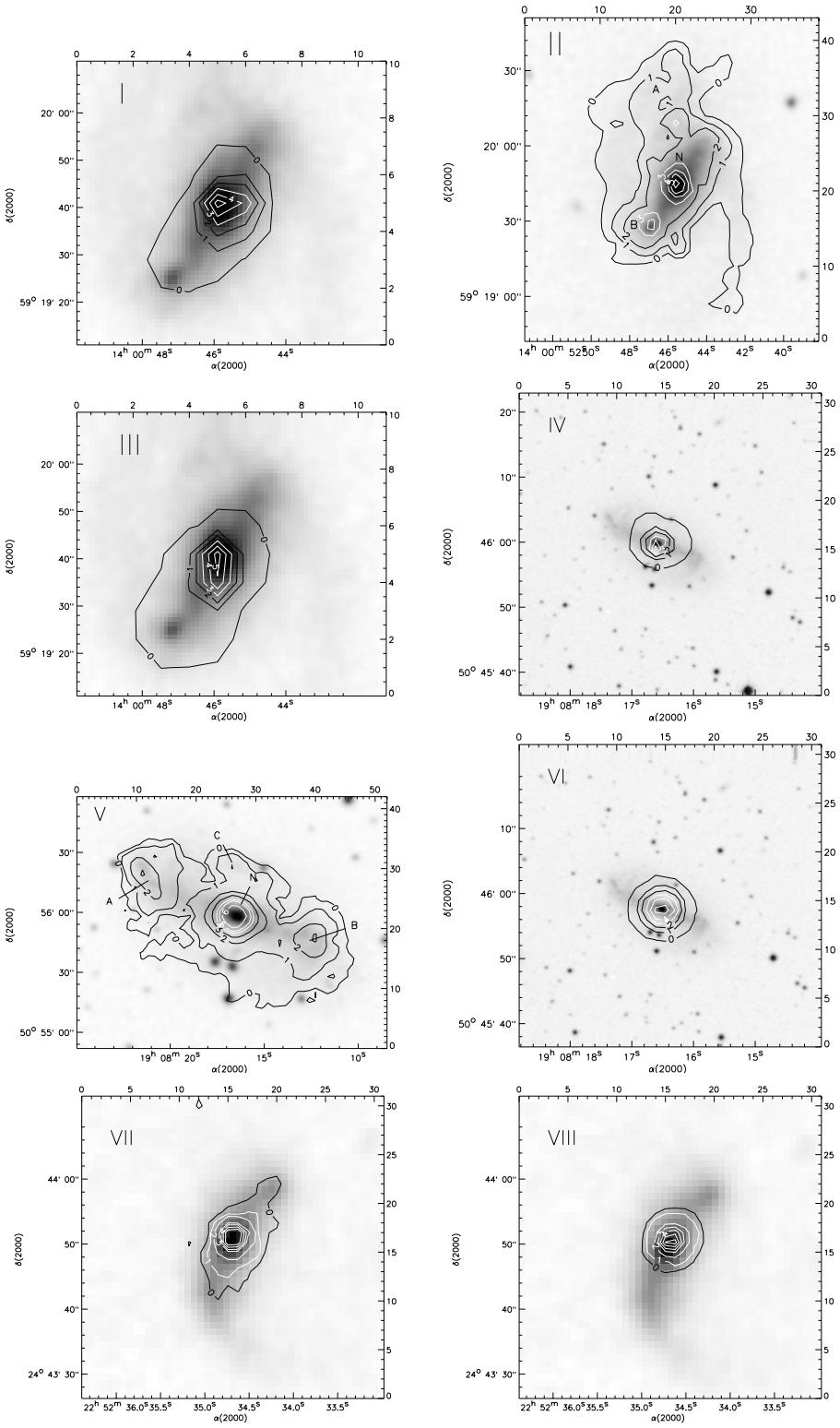

Fig. 1. ISOCAM maps of NGC 5430 (**I**) at 6.7 μm, **II**) at 12 μm, **III**) at 14.3 μm), NGC 6764 (**IV**) at 6.7 μm, **V**) at 12 μm, **VI**) at 14.3 μm) and Mrk 309 (**VII**) at 7.7 μm, **VIII**) at 14.3 μm), all overlaid on DSS images. For NGC 5430, the contour levels in the order 0 to 5 are as follows (in units of mJy/arcsec^2): **I**) 0.7, 1.5, 2.3, 3.2, 3.9, 4.8; **II**) 1.9, 3.5, 5.0, 6.5, 8.0, 9.5; **III**) 0.7, 2.1, 3.9, 6.1, 8.7, 11.4. For NGC 6764, the contour levels in the order 0 to 5 are as follows (in units of mJy/arcsec^2): **IV**) 0.6, 1.9, 3.1, 4.4, 5.7, 7.0; **V**) 1.0, 2.9, 4.9, 6.9, 8.8, 10.8; **VI**) 0.6, 2.3, 4.3, 7.5, 11.2, 16.1. For Mrk 309, the contour levels in the order 0 to 5 are as follows (in units of mJy/arcsec^2): **VII**) 0.2, 0.5, 0.9, 1.2, 1.5, 1.9; **VIII**) 0.2, 0.6, 1.3, 2.0, 2.8, 4.0. The top and right-hand scales refer to local pixel number scales.

Table 3. Fluxes for the galaxies observed by ISOCAM. A photometric uncertainty of 15% was assumed.

Reference wavelength $\lambda_{\rm ref}$	6.7 μm	7.7 μm	12.0 μm	14.3 μm
Wavelength range $\Delta\lambda$	5.0–8.5 μm	7.0–8.5 μm	8.0–15.0μm	12.0–18.0 μm
	Flux [mJy]	Flux [mJy]	Flux [mJy]	Flux [mJy]
NGC 5430	218 ± 26	–	459 ± 65	441 ± 68
NGC 6764	160 ± 24	–	310 ± 47	417 ± 63
Mrk 309	–	74 ± 11		160 ± 24

3.1.2. NGC 6764

Deconvolved 6.7, 12 and 14.3 μm maps of NGC 6764 overlaid on a DSS image are presented in Figs. 1(IV), (V) and (VI). Four infrared sources were detected on the higher resolution 12 μm map and are labelled A, B, C and N. The weaker sources A and B are probably associated with star formation regions in the arms of the galaxy, while C may also be a star formation region or an external galaxy. The derived ISOCAM fluxes are given in Table 3.

3.1.3. Mrk 309

The 7.7 and 14.3 μm maps of Mrk 309 are presented in Figs. 1(VII) and 1(VIII). Due to the low signal to noise ratio of the 7.7 μm image, deconvolution was not reliable. The nucleus of Mrk 309 was detected in both maps, though more weakly at 7.7 μm than at 14.3 μm. At low flux levels the 7.7 μm contours follow the outline of the galaxy, while the 14.3 μm emission is more compact. The ISOCAM infrared fluxes are given in Table 3.

3.1.4. VII Zw 19

No observations of VII Zw 19 were performed using ISOCAM.

3.2. PHT-S spectra

3.2.1. NGC 5430

The PHT-SL spectrum of the nuclear region of NGC 5430 is presented in Fig. 2a. The main PAH bands at 6.2, 7.7, 8.6 and 11.3 μm were easily detected, along with the [ArII] 6.99 μm feature. Two additional PHT-SL spectra of the regions labelled A and B were also obtained and are presented in Figs. 2b and 2c. In both spectra the PAH bands plus [ArII] at 6.99 μm were well detected, along with a blend of features at 10.6 μm in region A. The fluxes for the identified features are given in Table 4.

3.2.2. NGC 6764

Three PHT-SL spectra of the nucleus and regions A and B were obtained and are presented in Figs. 2d–2f. The main PAH bands at 6.2, 7.7, 8.6 and 11.3 μm were easily detected in the nuclear region, though only weakly detected at star formation region A. The spectrum of region B was very noisy and no features were reliably identified. The fluxes for the identified features are given in Table 5.

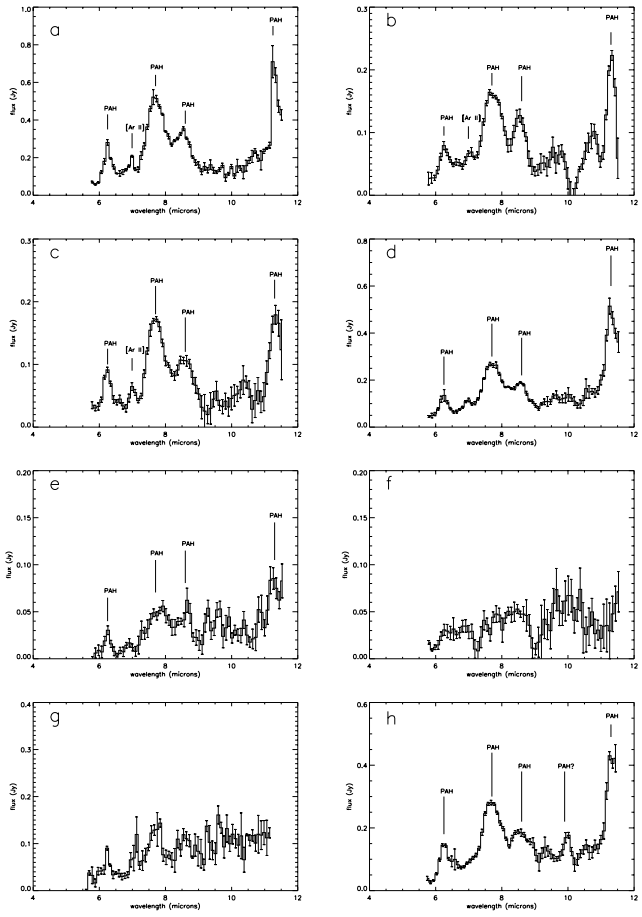

Fig. 2. PHT-SL spectra of NGC 5430 (**a)** the nucleus, **b)** region A, **c)** region B), NGC 6764 (**d)** the nucleus, **e)** region A, **f)** region B), Mrk 309 **g)** and VII Zw 19 **h)**. The PAH features and ionic lines are indicated.

3.2.3. Mrk 309

The PHT-SL spectrum of Mrk 309, shown in Fig. 2g was very noisy with no reliable detections of the PAH emission bands, and thus flux determinations were not made for features in this spectrum.

Table 4. PHT-SL line intensities for NGC 5430. The five columns give the target, the line identification, the reference wavelength, the wavelength range and the integrated flux respectively.

Target	Line ID	λ [μm]	$\Delta\lambda$ [μm]	Flux ($\times 10^{-15}$ W/m^2)
NGC 5430 Nucleus	PAH 6.2	6.2	5.8–6.6	6.98 ± 0.45
	ArII 6.99	6.99	6.8–7.1	2.17 ± 0.10
	PAH 7.7	7.7	7.2–8.2	13.84 ± 0.49
	PAH 8.6	8.6	8.2–9.0	5.88 ± 0.43
	PAH 11.3	11.3	11.0–11.6	8.88 ± 0.76
NGC 5430 Region A	PAH 6.2	6.2	6.0–6.4	1.24 ± 0.22
	ArII 6.99	6.99	6.8–7.1	0.59 ± 0.14
	PAH 7.7	7.7	7.2–8.2	4.14 ± 0.64
	PAH 8.6	8.6	8.4–9.1	1.09 ± 0.45
	PAH 11.3	11.3	11.0–11.6	1.61 ± 0.45
NGC 5430 Region B	PAH 6.2	6.2	6.0–6.4	1.01 ± 0.23
	ArII 6.99	6.99	6.8–7.1	0.51 ± 0.10
	PAH 7.7	7.7	7.2–8.2	4.33 ± 0.45
	PAH 8.6	8.6	8.4–9.1	1.99 ± 0.39
	SIV 10.51	10.51	10.4–10.8	0.32 ± 0.08
	PAH 11.3	11.3	11.0–11.6	1.42 ± 0.55

Table 5. PHT-SL line intensities for NGC 6764 and VII Zw 19 determined assuming a local continuum. The five columns give the target, the line identification, the reference wavelength, the wavelength range and the integrated flux respectively.

Target	Line ID	λ [μm]	$\Delta\lambda$ [μm]	Flux ($\times 10^{-15}$ W/m^2)
NGC 6764 Nucleus	PAH 6.2	6.2	5.8–6.6	6.31 ± 0.40
	PAH 7.7	7.7	7.2–8.2	8.14 ± 0.51
	PAH 8.6	8.6	8.2–9.0	2.82 ± 0.43
	PAH 11.3	11.3	11.0–11.6	0.0 ± 0.79
NGC 6764 Region A	PAH 6.2	6.2	6.0–6.4	0.87 ± 0.24
	PAH 7.7	7.7	7.2–8.2	1.73 ± 0.44
	PAH 8.6	8.6	8.4–9.1	0.91 ± 0.34
	PAH 11.3	11.3	11.0–11.6	0.67 ± 0.22
VII Zw 19	PAH 6.2	6.2	5.8–6.6	3.12 ± 0.28
	ArII 6.99	6.99	6.8–7.1	1.23 ± 0.12
	PAH 7.7	7.7	7.2–8.2	8.02 ± 0.53
	PAH 8.6	8.6	8.3–8.9	2.55 ± 0.34
	PAH? 9.7	9.7	9.4–10.0	2.73 ± 0.32
	PAH 11.3	11.3	11.0–11.6	3.55 ± 0.52

3.2.4. VII Zw 19

The PHT-SL spectrum of the nucleus of VII Zw 19 is presented in Fig. 2h. The main PAH bands at 6.2, 7.7, 8.6 and 11.3 μm are easily detected, along with [ArII] at 6.99 μm and a possible S(3) pure rotational line, υ = 0–0, of molecular hydrogen at 9.7 μm. The feature at 10.65 μm may be a blend of features. The identified line features and line fluxes are given in Table 5.

3.3. LWS spectra

The LWS spectra for the far-infrared lines [OI] at 63 μm and [CII] at 158 μm for both NGC 5430 and NGC 6764 are

Table 6. LWS line-fluxes for NGC 5430 and NGC 6764. The four columns give the species, the wavelength of the line and the line fluxes for each galaxy respectively.

Species	$\lambda_{\rm ref}$ (μm)	NGC 5430 Line flux ($\times 10^{-15}$ W/m^2)	NGC 6764 Line flux ($\times 10^{-15}$ W/m^2)
[O I]	63.1	7.5 ± 0.9	5.8 ± 0.7
[C II]	157.7	11.2 ± 1.3	10.3 ± 1.1

Table 7. Fluxes measured with LWS, binned to yield a single number per LWS detector.

Detector label	$\lambda_{\rm ref}$ (μm)	NGC 5430 Flux density (Jy)	NGC 6764 Flux density (Jy)
SW1	46.8	10.3	8.4
SW2	56.0	9.1	8.5
SW3	63.7	9.4	8.7
SW4	74.4	13.1	8.3
SW5	83.3	13.3	9.1
LW1	97.2	20.5	13.4
LW2	115.7	15.2	11.0
LW3	137.8	9.5	9.9
LW4	156.9	10.5	10.6
LW5	175.2	10.0 UL	7.7

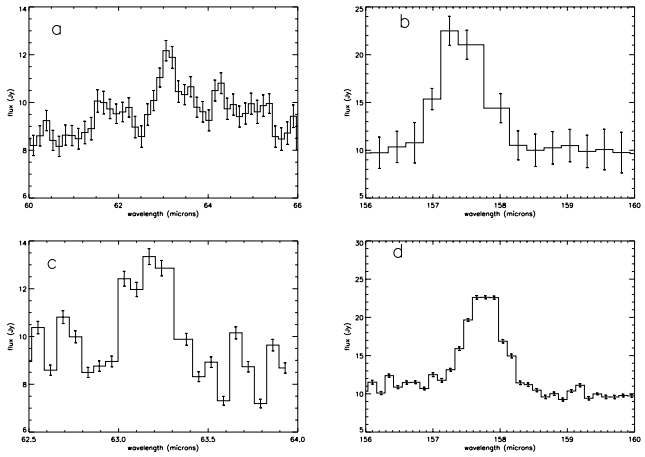

Fig. 3. LWS detections of the [OI] 63 μm and 158 μm lines from NGC 5430 (**a**), **c**)) and NGC 6764 (**b**), **d**)).

presented in Fig. 3, while the line fluxes are listed in Table 6. The continuum source strength, or applicable upper-limits, recorded in the ten LWS detectors by binning data across the spectral range of each detector are listed in Table 7.

4. Discussion

4.1. Previous surveys

4.1.1. NGC 5430

Keel (1982) estimated that $\sim 5 \times 10^3$ WN7 stars and $\sim 10^4$ WC8 stars reside in this knot as well as a still larger number of O stars. With improved spectra Keel (1987) later claims that though HeII λ4686 and [NIII] λ4640 are detected, [CIV] is not and therefore the WR stars in the knot might be regarded as some species of WN stars. Keel (1987) also identifies 26 other "normal" HII regions present in NGC 5430 other than the southeast knot and the nucleus.

According to Keel (1987) the observed star formation in the SE knot is both sudden and transient. The nebula is expanding, probably driven by stellar winds, and dissipating on a timescale of $\sim 10^7$ years. Star formation elsewhere in the galaxy appears to be proceeding at a normal rate and with a normal HII region luminosity function (Keel 1987). The nebular abundances in the SE knot are rather high for a position so far out in a disk or bar and are more like those seen in nuclei. This suggests that this knot might be a separate object resulting from the collision of a dwarf irregular galaxy with the disk and bar of NGC 5430. Furthermore, the Hα luminosity and emission-line ratios are quite comparable to those seen in such systems as Mrk 108 (Keel et al. 1985). Using starburst models by Cervino & Mas-Hesse (1994) and Leitherer & Heckman (1995), Contini et al. (1996) estimated the age of the starburst in the SE knot to be 3 Myr and 4 Myr respectively. For the nucleus the estimates are 8 Myr and 9 Myr respectively. These estimates are certainly compatible with the scenario of separate star formation mechanisms in the nucleus and SE knot of NGC 5430.

4.1.2. NGC 6764

Osterbrock & Cohen (1982) detected WR emission features in the spectrum of the nucleus of this narrow emission line galaxy. From the equivalent widths of the WR emission features at 4650 Å, Osterbrock & Cohen (1982) estimate that the number of WN and WC stars is 5.0×10^4 and 9.0×10^4 respectively.

Confirmation of the existence of the WR features detected by Osterbrock & Cohen (1982) was made by Eckart et al. (1996), who claim that the number of WO stars is negligible and WN stars dominate the WR star population. Detection of the broad [CIII] λ5696 and [CIV] λ5808 lines by Kunth & Contini (1999) indicate the existence of some WC stars. Eckart et al. (1996) estimate that there are a total of 3600 WR stars contributing to the ionizing flux in the nucleus of NGC 6764. These authors also note that the WR feature is spatially extended and most of it originates in the 1.6″ diameter nuclear optical continuum source. Using the same method as for NGC 5430, Contini et al. (1996) estimates the age of the starburst in the nucleus of NGC 6764 to be 5.0 Myr and 6.5 Myr depending on which models are used (Cervino & Mas-Hesse 1994; Leitherer & Heckman 1995). The presence of WR stars (Osterbrock & Cohen 1982) indicates that the starburst is very young (≤6 Myr) and that many massive stars were born during the burst. Eckart et al. (1996) conclude that the nucleus of NGC 6764 has recently undergone or is currently undergoing an intense starburst with a characteristic timescale of a few times 10^7 years.

4.1.3. Mrk 309

Arkelian et al. (1972) noted the presence of diffuse Hα emission, as well as the lines NII $\lambda\lambda$6548, 6583. The presence of these lines were later confirmed by Afanasev et al. (1980). Osterbrock & Cohen (1982) detected a blend of three broad emission features at 4650 Å in the nucleus of this galaxy: NIII λ4640, CIV λ4660 and HeII λ4686. These lines are slightly narrower than in NGC 6764 and hence a slightly lower proportion of the continuum radiation at 4650 Å comes from WR stars. However, Conti (1991) argues that the emission feature at 4660 Å is attributable to FeIII rather than CIV, and is consistent with the deficiency in the strength of the CIII λ4650 emission feature as noted by Osterbrock & Cohen (1982). CIV λ5808 and CIII λ5696 emission, attributed to WC stars, has also been tentatively detected (Osterbrock & Cohen 1982). From the equivalent widths of the WR emission features at 4650 Å these authors deduced that 9% of the continuum radiation at this wavelength comes from WR stars and hence calculated the number of WN and WC stars to be approximately 0.9×10^4 and 1.5×10^4 respectively.

With the exception of the WR features at 4650 Å, Osterbrock & Cohen (1982) point out that the emission line spectra of Mrk 309 is typical of low-ionization galaxies with gas in their nuclei apparently photoionized by early-type stars, as in HII regions. Indeed Mazzarella & Balzano (1986) places Mrk 309 in the HII spectral class. Osterbrock & Cohen (1982) concluded that the number of O stars in Mrk 309 is comparable to the number of WR stars and hence massive star formation must have occurred recently.

4.2. Dust components and luminosities

There is growing evidence for the existence of several components within the dust distribution of galaxies (Klaas et al. 2001). Specifically this can be divided into warm dust components associated with star formation regions and a spatially extended distribution of cold dust. Warm dust emission is generally associated with very small dust grains which are heated by the single-photon absorption process to temperatures up to several hundred Kelvin (Desert et al. 1990), and are not in thermal equilibrium with their environment (Calzetti et al. 2000). Emission from very small dust grains account for the characteristics of the mid-IR at wavelengths ≤40 μm. The cold dust emission is associated with classical large grains, emitting at wavelengths in excess of 80 μm in thermal equilibrium with their environment (Calzetti et al. 2000). The large grains are heated by the normal interstellar radiation field. These large dust grains account for practically all the emission longward of 80 μm in galaxies.

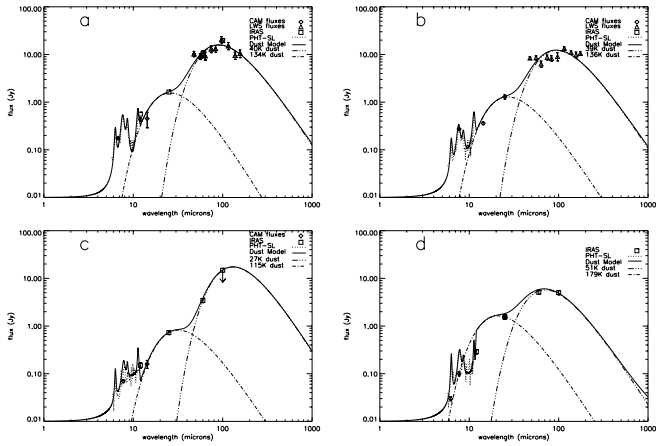

Fig. 4. Spectral energy distribution of **a)** NGC 5430, **b)** NGC 6764 **c)** Mrk 309 and **d)** and VII Zw 19 using ISO and IRAS flux data, including the key for the different symbols. The models are described in the text.

To model the dust continuum at mid and far-infrared wavelengths, modified blackbody functions comprised of a greybody component were fitted to the IRAS and ISO fluxes for the galaxies in the WR sample. The spectral energy distributions of NGC 5430, NGC 6764, Mrk 309 and VII Zw 19 using IRAS, ISOCAM, PHT-SL and LWS fluxes are presented in Figs. 4a–d. The dust model, denoted by the solid curve was fitted to the data and contains two separate dust populations along with the PAH bands (Boulanger et al. 1998): a warm dust component at 115–179 K and a cooler dust component at 27–64 K and each component is indicated in Figs. 4a–d.

For VII Zw 19 at $\lambda \geq 300$ μm, it is noticeable that the emission is flattening, possibly due to the presence of a very cold dust component. However overall, the results are consistent with similar modelling by Siebenmorgen et al. (1999).

To determine the mass of each dust component, several parameters need to be determined. The luminosity of each component was determined from the integrated fluxes of each greybody, along with the dust temperature and then a dust mass for each component was determined (Klaas et al. 2001). Using this method, the IR luminosities and dust component masses in similar starburst galaxies such as the Antennae and NGC 6240 were determined in order to check the validity of the derived values (Klaas et al. 1997).

Table 8. Dust luminosities and masses.

Galaxy	$T_{\rm warmdust}$ (K)	$T_{\rm cooldust}$ (K)	$L_{\rm IR}$ (ISO) $[L_\odot]$	$L_{\rm IR}$ (IRAS) $[L_\odot]$
Mrk 309	143	64	1.40×10^{11}	3.58×10^{11}
NGC 5430	134	40	5.55×10^{10}	8.78×10^{10}
NGC 6764	136	39	2.85×10^{10}	3.53×10^{11}
VII Zw 19	179	51	7.35×10^{10}	1.07×10^{11}

Table 9. Star formation/AGN diagnostic ratios using CAM and PHT-S data.

Galaxy	14.3/6.75 μm	14.3/7.7 μm	F(PAH 7.7 μm)/ F(7.7 μm continuum)	L(PAH)/ L(40–120 μm)
Mrk 309	2.16	2.2	5.78	–
NGC 5430	2.57	2.1	4.79	0.091
NGC 6764	2.60	2.0	1.22	0.088
VII Zw 19	–	–	4.82	0.122

For each target, the luminosity for the galaxy, the dust component luminosity and the derived dust masses are given in Table 8. For the warm and cool dust components, the derived values are quite similar to starbursts such as the Antennae, NGC 6240 (Klaas et al. 1997), NGC 1741 (O'Halloran et al. 2002) and Mrk 297 (Metcalfe et al. 2005).

4.3. Current star formation

4.3.1. Diagnostics using ISOCAM data

In order to determine the current state of star formation within our sample, diagnostics such as the 14.3/6.75 μm flux ratio can be used as they act as standard ratio diagnostics for this type of investigation (Vigroux et al. 1999; Helou 1999). Since the 14.3 μm flux is dominated primarily by emission from very small dust grains and the 6.75 and 7.7 μm fluxes are dominated by PAHs, the 14.3/7.7 μm ratio provides a diagnostic similar to the 14.3/6.75 μm ratio, allowing a determination of the current state of the starburst. These diagnostic ratios generally decrease as interactions develop and starbursts age (Vigroux et al. 1999; Helou 1999) – the highly ionizing O stars in the burst die off, thus no longer destroying nearby PAHs, plus emission from nearby dust heated by massive stars also decreases. For the three galaxies with available ISOCAM data, the derived ratios are given in Table 9. The 6.7 μm flux for Mrk 309 was synthesized from the PHT-SL data, a technique used previously when faced with the lack of 6.75 μm ISOCAM data (O'Halloran et al. 2000, 2002). The obtained 14.3/7.7 14.3/6.75 and 14.3/7.7 μm ratios were indicative of strong ongoing star formation, with ratios generally well above 2, similar to those found in earlier works for strong starbursts (Vigroux et al. 1999).

4.3.2. Star formation rate

Using the calibrations in Kennicutt (1998) and Wilke et al. (2004), we can calculate the global star formation rate for the sample from the derived IR luminosities. Global SFRs of 9.6, 5.0, 24.1 and 12.6 $M_\odot$ yr^{-1} were calculated for NGC 5430, NGC 6764, Mrk 309 and VII Zw 19 respectively. These strong levels of ongoing star formation are consistent with the values from the infrared diagnostics.

4.4. Do any galaxies within the sample harbour an AGN?

4.4.1. Mid-IR diagnostics

Historically, 2 galaxies of the sample have been suspected of harbouring AGN. Mrk 309 was identified as a galaxy with a bright UV continuum and noticeable Hα emission by Markarian (1971) who noted the possibility of a Seyfert nucleus. Afanasev (1980) reported Hα and [NII] λ6548, λ6583 and stated that Mrk 309 may be a Seyfert 2 galaxy. NGC 6764 has been classified as a LINER galaxy based on optical spectroscopy (Osterbrock & Cohen 1982). NIR spectroscopy of the nuclear region (Schinnerer et al. 2000) reveals that star formation is confined to two regions, one with a radius less than 100 pc containing the WR stars. NGC 6764 also shows strong variations in ROSAT X-ray flux density by at least a factor of 2 on timescales of 7 days (Schinnerer et al. 2000), suggesting the presence of a compact AGN with $R \sim 10^3$ AU. No previous survey has suggested that NGC 5430 or VII Zw 19 harbours an AGN.

In order to test the possibility that the central region harbours an AGN, diagnostic tools using ISO data are available to probe the nature of the activity within the central starburst region. The ratio of the integrated PAH luminosity and the 40 to 120 μm IR luminosity (Lu et al. 1999) discriminates between starbursts, AGN and normal galaxies. The lower the ratio, the more likely the galaxy harbours an AGN, due to high very small dust grain emission powered by AGN longward of 10 and shorter than 50 μm, plus PAH destruction near the AGN (Vigroux et al. 1999). Similarly, the ratio of the 7.7 μm PAH flux to the continuum level at this wavelength can provide a measure of the level of activity within the

nucleus (Genzel et al. 1998; Clavel et al. 2000; Laureijs et al. 2000), as a high ratio indicates the lack of an AGN excited dust component. The derived ratio values are given in Table 9 for each galaxy. Given the high L(PAH)/L(40–120 μm) and F(PAH 7.7 μm)/F(7.7 μm continuum) values, it can be stated that most of these galaxies are home to only a compact burst of star formation and that an AGN is not required within the central bursts. – values of ≤1.5 and 0.06 would be indicative of a strongly dominant AGN component. The exception is NGC 6764, whose F(PAH 7.7 μm)/F(7.7 μm continuum) value of 1.22 is consistent with the presence of an AGN, yet the L(PAH)/L(40–120 μm) is more in line with a starburst, a finding which suggests the presence of a compact AGN dominated by a strong starburst component.

4.4.2. Far-IR diagnostics

Atomic oxygen and ionized carbon are the principal coolants of the gaseous interstellar medium via their fine structure lines in the far infrared (FIR). In particular, [OI] at 63 μm and [CII] at 158 μm dominate the cooling in the photodissociation regions associated with massive stars such as Wolf Rayets, along with [OI] at 146 μm and [OIII] at 88 μm (Malhotra et al. 1997). The [OI] and [CII] features are also produced in the warm atomic gas behind dissociative shocks, in HII regions or in photodissociation regions (PDRs), while [OIII] is more associated with denser environments within HII regions (Malhotra et al. 1997; Braine & Hughes 1999).

The [OI] 63 μm and [CII] 158 μm lines were well detected in both NGC 5430 and NGC 6764 and allowed a determination of the $L_{\rm CII}/L_{\rm FIR}$ and $(L_{\rm CII}+L_{\rm OI})/L_{\rm FIR}$ ratios, which could be used to probe the nature of the environment within the galaxy. For NGC 5430, values of $L_{\rm CII}/L_{\rm FIR}$ = 1.9×10^{-3} and $(L_{\rm CII}+L_{\rm OI})/L_{\rm FIR}$ = 1.1×10^{-2} were determined, given an IRAS flux ratio $F(60\ \mu{\rm m})/F(100\ \mu{\rm m})$ = 0.55. For NGC 6764, values of $L_{\rm CII}/L_{\rm FIR}$ = 2.9×10^{-3} and $(L_{\rm CII}+L_{\rm OI})/L_{\rm FIR}$ = 1.9×10^{-2} were determined, given an IRAS flux ratio $F(60\ \mu{\rm m})/F(100\ \mu{\rm m})$ = 0.53. The $L_{\rm CII}/L_{\rm FIR}$ and $(L_{\rm CII}+L_{\rm OI})/L_{\rm FIR}$ ratios are consistent with those from other starburst galaxies, given an IRAS flux ratio $F(60\ \mu{\rm m})/F(100\ \mu{\rm m})$ = 0.66 (Malhotra et al. 1997; Braine & Hughes 1999), though for higher dust temperatures and star formation rates these ratios decrease (Malhotra et al. 1997).

5. Conclusions

Observations of four of a sample of WR galaxies using the Infrared Space Observatory were presented in this paper. ISOCAM maps of NGC 5430, Mrk 309 and NGC 6764 revealed the location of star formation regions in each galaxy, while ISOPHOT spectral observations from 4 to 12 μm detected the ubiquitous PAH bands in the nuclei of the targets, and several of the disk star forming regions. Strong [OI] and [CII] lines were detected in LWS spectra of NGC 5430 and NGC 6764.

Using a combination of ISO and IRAS flux densities, a dust model based on the sum of two modified blackbody components were successfully fitted to the available data. The modified blackbody functions were comprised of a $1/\lambda$ component with temperatures of 27–64 K and 115–179 K depending on the galaxy. These models accounted for the far-infrared emission and were then used to calculate new values for the total IR luminosities for each galaxy and the size of the various dust populations. For the dust components, the derived values are quite similar to starbursts such as the Antennae and Mrk 297.

The high ISOCAM flux ratios are indicative of strong, ongoing star formation in these galaxies. The high L(PAH)/L(40–120 μm) and F(PAH 7.7 μm)/F(7.7 μm continuum) values also state that most of these galaxies are home to only a compact burst of star formation and that an AGN is not required within the central bursts. The exception however is NGC 6764, whose F(PAH 7.7 μm)/F(7.7 μm continuum) value of 1.22 is consistent with the presence of an AGN, yet the L(PAH)/L(40–120 μm) is more in line with a starburst, a finding in line with a compact AGN dominated by the starburst.

Acknowledgements. The ISOCAM data presented in this paper was analyzed using "CIA", a joint development by the ESA Astrophysics Division and the ISOCAM Consortium. The ISOCAM Consortium is led by the ISOCAM PI, C. Cesarsky, Direction des Sciences de la Matière, CEA, France. The ISOPHOT data presented in this paper was reduced using PIA, which is a joint development by the ESA Astrophysics Division and the ISOPHOT consortium. The ISO Spectral Analysis Package (ISAP) is a joint development by the LWS and SWS Instrument Teams and Data Centers. Contributing institutes are CESR, IAS, IPAC, MPE, RAL and SRON.

References

Abergel, A., Bernard, J. P., Boulanger, F., et al. 1996, A&A, 315, L329
Acosta-Pulido, J. A., Gabriel, C., & Castaeda, H. 2000, Exp. Astron., 10, 333
Afanasev, V. L., Lipovetskii, V. A., Markarian, B. E., et al. 1980, Astrofiz., 16, 193
Allen, D. A., Wright, A. E., & Goss, W. M. 1976, MNRAS, 177, 91
Arkelian, M. A., Dibai, E. A., & Episov, V. F. 1972, Astrofiz., 8, 177
Aussel, H., Cesarsky, C. J., Elbaz, D., et al. 1999, A&A, 342, 313
Beck, S. C. 2000, AJ, 120, 244
Beck, S. C., Garrington, S. T., Turner, J. L., & Van Dyk, S. D. 2004 [arXiv:astro-ph/0406560]
Blommaert, J., Siebenmorgen, R., Coulais, A., et al. 2001, ISO Handbook, Vol. II: The ISO Camera, ESA, SP-1262, http://www.iso.vilspa.esa.es/manuals
Boulanger, F., Boissel, P., Cesasrsky, D., et al. 1998, A&A, 339, 194
Braine, J., & Hughes, D. H. 1999, A&A, 344, 779
Calzetti, D., Armus, L., Bohlin, R. C., et al. 2001, AJ, 533, 682
Cervino, M., & Mas-Hesse, J. M. 1994, A&A, 284, 749
Clavel, J., Schulz, B., Altieri, B., et al. 2000, A&A, 357, 839
Condon, J. J., Condon, M. A., Gisler, G., et al. 1982, ApJ, 252, 102
Conti, P. S. 1991, ApJ, 377, 115
Conti, P. S., & Vacca, W. D. 1994, ApJ, 423, L97
Contini, T. 1996, in WR Stars in the Framework of Stellar Evolution, ed. J. M. de Vreux et al., 33rd Liège Int. Astroph. Coll., Liège, Université de Liège, 619
Delaney, M., & Ott, S. 2002, ISOCAM Interactive Analysis User's Manual, Version 5.0, SAI/96-5226/Dc, http://www.iso.vilspa.esa.es/users/expl_lib/CAM_top.html

Desert, F., Boulanger, F., & Puget, J. L. 1990, A&A, 237, 215
Eckart, A., Cameron, M., Boller, T., et al. 1996, ApJ, 472, 588
Gabriel, C. 2002, PHT Interactive Analysis User Manual, ESA, http://www.iso.vilspa.esa.es/manuals/
Genzel, R., Lutz, D., Sturm, E., et al. 1998, ApJ, 498, 579
Gry, C., Swinyard, B. M., Harwood, A., et al. 2003, ISO Handbook, Vol. III: LWS – The Long-Wavelength Spectrometer, ESA, SP-1262, http://www.iso.vilspa.esa.es/manuals
Heckman, T. M. 1980, A&A, 87, 152
Helou, G. 1999, in The Universe as seen by ISO, ed. P. Cox, & M. F. Kessler, ESA SP-427, 2, 797
Keel, W. C. 1982, PASJ, 94, 765
Keel, W. C., Kennicutt, R. C., Hummel, E., et al. 1985, AJ, 90, 708
Keel, W. C. 1987, A&A, 172, 43
Kennicutt, R. C. 1998, ApJ, 498, 541
Kessler, M. F., Muller, T. G., Leech, K., et al. 2003, ISO Handbook, Vol. I: ISO – Mission & Satellite, ESA, SP-1262, http://www.iso.vilspa.esa.es/manuals
Klaas, U., Haas, M., Heinrichsen, I., & Schulz, B. 1997, A&A, 325, 21
Klaas, U., Haas, M., Muller, S. A. H., et al. 2001, A&A, 379, 823
Kunth, D., & Joubert, M. 1985, A&A, 142, 411
Kunth, D., & Contini, T. 1999, in Wolf-Rayet stars as tracing the AGN-starburst connection, 725
Laureijs, R., Watson, D., Metcalfe, L., et al. 2000, A&A, 359, 900
Laureijs, R. J., Klaas, U., Richards, P. J., et al. 2003a, ISO Handbook, Vol. IV: PHT – The Imaging Photo-Polarimeter, ESA, SP-1262, http://www.iso.vilspa.esa.es/manuals
Laureijs, R. J., Klaas, U., Richards, P. J., et al. 2003b, ISOPHOT Data Users Manual, ESA, http://www.iso.vilspa.esa.es/manuals/
Leitherer, C., & Heckman, T. M. 1995, ApJS, 96, 9
Lemke, D., Klaas, U., Abolins, J., et al. 1996, A&A, 315, 64
Li, W., Modjaz, M., Treffers, R. R., & Filippenko, A. V. 1998, IAUC, 6850
Lu, N. Y., Helou, G., Silbermann, N., et al. 1999, in The Universe as seen by ISO, ed. P. Cox, & M. F. Kessler, ESA SP-427, 2, 929
Malhotra, S., Helou, G., Stacey, G., et al. 1997, ApJ, 491, 27
Maeder, A., & Conti, P. S. 1994, ARA&A, 32, 227
Markarian, B. E., & Lipovetskii, V. A. 1971, Astrofiz., 7, 511
Mazzarella, J. M., & Balzano, V. A. 1986, ApJS, 62, 751
Metcalfe, L., O'Halloran, B., McBreen, B., et al. 2005, A&A, submitted
Meurer, G. R., Heckman, T. M., Leitherer, C., et al. 1995, AJ, 110, 2665
O'Halloran, B., Metcalfe, L., Delaney, M., et al. 2000, A&A, 360, 871
O'Halloran, B., Metcalfe, L., McBreen, B., et al. 2002, ApJ, 575, 747
O'Halloran, B., Steel, S., Metcalfe, L., et al. 2005, A&A, submitted
Okumura, K. 1998, ISOCAM PSF Report, http://www.iso.vilspa.esa.es/
Osterbrock, D. E., & Cohen, R. D. 1982, ApJ, 261, 64
Ott, S., Abergel, A., Altieri, B., et al. 1997, in Astronomical Data Analysis Software and Systems VI, ed. G. Hunt, & H. Payne, ASP Conf. Ser., 125, 34
Rubin, V. C., Thonnard, N. C., & Ford, W. K. 1975, ApJ, 199, 31
Siebenmorgen, R., Krugel, E., & Chini, R. 1999, A&A, 351, 495
Schaerer, D., Contini, T., & Pindao, M. 1999, A&AS, 136, 35
Schinnerer, E., Eckart, A., & Boller, T. 1999, AJ, 545, 205
Sidher, S. D., Swinyard, B. M., Harwood, A. S., et al. 1997, in Proc. the first ISO workshop on Analytical Spectroscopy, Madrid, Spain, 6–8 October, ed. A. M. Heras, K. Leech, N. R. Trams, & M. Perry, ESA SP-419, 297
Sidher, S. D., Griffin, M. J., Davis, G. R., et al. 2000, Icarus 147, issue 1, 35
Starck, J. L., Murtagh, F., & Bijaoui, A. 1998, in image processing and data analysis. The multiscale approach (Cambridge, UK: Cambridge University Press), ISBN: 0521590841
Steel, S., Smith, N., Metcalfe, L., Rabbette, M., & McBreen, B. 1996, A&A, 311, 721S
Stevens, I. R., & Strickland, D. K. 1998, MNRAS, 294, 523
Swinyard, B. M., Burgdorf, M. J., Clegg, P. E., et al. 1998, in Infrared Astron. Instrumentation, ed. A. M. Fowler, Proc. SPIE, 3354, 888
Swinyard, B. M., Clegg, P. E., Leeks, S., et al. 2000, Exp. Astron., 10, 157
Thuan, T. X., & Gunn, J. E. 1976, PASP, 88, 543
Vigroux, L., Charmandaris, V., Gallais, P., et al. 1999, in The Universe as seen by ISO, ed. P. Cox, & M. F. Kessler, ESA SP-427, 2, 805
Vitores, A. G., Zamorano, J., Rego, M., et al. 1996, A&AS, 118, 7
Wilke, K., Klaas, U., Lemke, D., et al. 2004, A&A, 414, 69
Zamorano, J., Rego, M., Gallego, J., et al. 1994, ApJS, 95, 387